Phosphoinositide Regulation of Integrin Trafficking Required for Muscle Attachment and Maintenance

Inês Ribeiro[1], Lin Yuan[2], Guy Tanentzapf[2], James J. Dowling[3], Amy Kiger[1]*

1 Section of Cell and Developmental Biology, University of California San Diego, La Jolla, California, United States of America, **2** Department of Cellular and Physiological Sciences, University of British Columbia, Vancouver, Canada, **3** Department of Pediatrics, University of Michigan Medical Center, Ann Arbor, Michigan, United States of America

Abstract

Muscles must maintain cell compartmentalization when remodeled during development and use. How spatially restricted adhesions are regulated with muscle remodeling is largely unexplored. We show that the myotubularin *(mtm)* phosphoinositide phosphatase is required for integrin-mediated myofiber attachments in *Drosophila melanogaster*, and that *mtm*-depleted myofibers exhibit hallmarks of human XLMTM myopathy. Depletion of *mtm* leads to increased integrin turnover at the sarcolemma and an accumulation of integrin with PI(3)P on endosomal-related membrane inclusions, indicating a role for Mtm phosphatase activity in endocytic trafficking. The depletion of Class II, but not Class III, PI3-kinase rescued *mtm*-dependent defects, identifying an important pathway that regulates integrin recycling. Importantly, similar integrin localization defects found in human XLMTM myofibers signify conserved *MTM1* function in muscle membrane trafficking. Our results indicate that regulation of distinct phosphoinositide pools plays a central role in maintaining cell compartmentalization and attachments during muscle remodeling, and they suggest involvement of Class II PI3-kinase in MTM-related disease.

Citation: Ribeiro I, Yuan L, Tanentzapf G, Dowling JJ, Kiger A (2011) Phosphoinositide Regulation of Integrin Trafficking Required for Muscle Attachment and Maintenance. PLoS Genet 7(2): e1001295. doi:10.1371/journal.pgen.1001295

Editor: Eric Rulifson, University of California San Francisco, United States of America

Received September 15, 2010; **Accepted** January 6, 2011; **Published** February 10, 2011

Copyright: © 2011 Ribeiro et al. This is an open-access article distributed under the terms of the Creative Commons Attribution License, which permits unrestricted use, distribution, and reproduction in any medium, provided the original author and source are credited.

Funding: This work was supported by funds to GT from NSERC discovery grant 356502, an HFSP Career Development Award, a CIHR New Investigator Award, and Michael Smith Foundation for Health Research Scholar Award and by funds awarded to AK from NIH GM078176, March of Dimes Basil O'Connor Award 5-FY06-598, Packard Foundation Fellowship 2005-29096, and Hellman Family Foundation Fellowship. The funders had no role in study design, data collection and analysis, decision to publish, or preparation of the manuscript.

Competing Interests: The authors have declared that no competing interests exist.

* E-mail: akiger@ucsd.edu

Introduction

Myofibers are large, highly differentiated contractile cells that rely on strong extracellular attachments to preserve their integrity during force-generating muscle contractions. Myofiber attachments are mediated by integrin adhesion complexes (IACs) composed of α- and β- transmembrane heterodimers that associate with cytoskeletal bridging factors, similar to those found in non-muscle cells [1]. IACs are crucial at myotendinous junctions (MTJs), attaching the ends of myofibers to tendons. In addition, IACs concentrated at costameres associated with repeating sarcomeric Z-lines attach peripheral myofibrils to the extracellular matrix. IACs are known to be essential for invertebrate and vertebrate muscle cell attachments and organization [2,3], but it is unclear how the critical pattern of spatially restricted adhesions is continuously maintained.

In non-muscle cells, integrin turnover through endocytic recycling has clear roles in localization of dynamic adhesion complexes that mediate cell migration and membrane remodeling in cytokinesis. Trafficking pathways that engage specific endocytic adaptors, protein kinases and Rab GTPases for internalization and recycling of specific integrins are emerging, as primarily understood in isolated cells [4]. In contrast, it is not clear how important regulated integrin turnover is in differentiated muscle, or how this turnover is regulated. In isolated myofibers, uptake of markers for endocytic recycling occurred in the vicinity of adhesion sites and trafficked to perinuclear compartments, distinct from a degradative pathway [5], suggesting common trafficking themes shared with non-muscle cells. Experiments using fluorescence recovery after photobleaching (FRAP) in intact flies recently provided the first observation of endocytosis-dependent, growth-regulated mobility of IAC proteins at MTJs [6], underscoring the significance of regulated endosomal integrin trafficking in muscles, as well.

Dynamic membrane compartment identity and functions are in part conveyed through phosphoinositides. Phosphoinositides exist as seven phosphorylated phosphatidylinositol forms interconverted by dedicated lipid kinases and phosphatases [7]. Different phosphoinositide forms can recruit specific binding proteins to distinct membranes in order to elicit spatiotemporal responses that include localized signaling, cytoskeletal reorganization, membrane deformation and trafficking. However, the complex cellular relationships in vivo are less defined.

The control of phosphoinositide balance by the Myotubularin (MTM) phosphoinositide phosphatases is both elaborate and crucial in metazoans. MTMs are encoded as a large family of genes (15 humans, 7 flies, 1 yeast) associated with human disease [8]. Mutations in human *MTM1* lead to human X-linked myotubular (centronuclear) myopathy (XLMTM, OMIM #310400) characterized by centrally misplaced nuclei in hypotrophic myofibers [9,10]. Disruption of related *MTMR2* leads to Charcot-Marie-Tooth neuropathy (CMT4B1, OMIM #601382) with abnormal morphology and plasma membrane outfolds in

Author Summary

Muscles require strong extracellular attachments to preserve cellular integrity during force-generating contractions. Integrin transmembrane receptors mediate muscle attachments at highly localized sites, but how this pattern of attachments is continuously maintained with muscle use is not understood. Human X-linked myotubular myopathy (XLMTM), a frequently fatal muscle disease, is associated with mutations in the *MTM1* lipid regulator. Myotubularin (MTM) lipid phosphatases are implicated in endocytosis, a process of cellular uptake that can traffic transmembrane receptors for redelivery to the plasma membrane or to protein destruction. Here, we address MTM roles in muscle, using the genetically tractable fruit fly for detailed investigation of muscle cellular organization and functions. We show that fly muscle cells depleted for *mtm* function exhibit hallmarks of human XLMTM. We found that *mtm* regulates integrin localization through endocytosis and, in this role, is needed to maintain muscle attachments. Co-depletion of Class II PI3-kinase with *mtm* restores normal integrin localization at muscle attachment sites and fly survival, identifying a potential therapy target in MTM-related disease. Importantly, we show that integrin localization is also disrupted in human XLMTM. Our work shows conservation of MTM function in integrin trafficking and reveals insights into regulation of muscle cell maintenance and human disease.

myelinating Schwann cells [11]. Both MTM1 and MTMR2 partially localize to endosomal compartments and are attributed with PI(3)P and PI(3,5)P_2 turnover [12–18]. However, it is not clear how disruption of MTMs and potential regulation of endosomal phosphoinositides might lead to the morphological defects found in MTM-related disease. The kinase(s) that coregulate the relevant phosphoinositide pool(s) for specific MTM functions in muscle have not been explored. Candidates include both Class II and Class III PI3-kinases (PI3KC2 and Vps34, respectively) that generate PI(3)P [19]. Vps34 has well established conserved roles at endosomal membranes. In contrast, PI3KC2 has less-understood roles mostly related with functions at the plasma membrane [18,20–23].

Here we show that *mtm* (GenBank NM_078765), encoding the sole *D. melanogaster* homolog of human MTM1/MTMR2, acts with Class II *Pi3K68D* (GenBank NM_079304) to maintain attachments upon myofiber remodeling. We found that *mtm* controls β-integrin turnover and trafficking from perinuclear compartments to maintain spatially restricted adhesions at MTJs and costameres, reflecting a broad *mtm* requirement for integrin-mediated adhesion also needed in the wing. The defects discovered in flies were substantiated by observing similar integrin mislocalization in human XLMTM myopathy, suggesting a conserved *MTM1* function in membrane trafficking and roles for integrin adhesions in maintenance of myofiber organization. Altogether, our results identify specific phosphoinositide regulation important for endocytic recycling and dynamic control of cell compartmentalization.

Results

Mtm is required to maintain myofibers during remodeling and for adult muscle function

Given the role for myotubularins in human myopathy, and our discovery of an *mtm* requirement in muscle essential for fly viability [18], we investigated the contribution of *mtm*-dependent phosphoinositide regulation to muscle cell function and compartmentalization. Loss of *mtm* function using either null alleles or muscle-directed RNAi had no visible effects on muscle in larvae, which remained mobile and exhibited normal body wall muscle formation, attachments and growth (Figure 1A and 1B–1B′, Figure S1A–S1C′). However, targeted RNAi depletion revealed muscle requirements for *mtm* at later developmental stages. Muscle-specific *mtm* knockdown, as indicated by protein depletion, showed either animal lethality (24B-GAL4) or developmental delay (DMef2-GAL4) around the stage of adult eclosion that was rescued by co-expression of either wildtype *mtm* or human *MTMR2* (Figure 1A and 1C, Figure S1B).

Metamorphosis occurs inside a rigid pupal case that adult flies escape at eclosion with the help of muscle contractions, including supporting contractions from a subset of abdominal persistent larval muscles (PLMs) [24,25]. The PLMs called dorsal temporary internal oblique muscles (IOMs) are large, individual, multinuceated myofibers that span abdominal segments (Figure 1D; Figure S1D). Consistent with defects in eclosion, there was a decrease in the number of both dorsal IOMs and ventral PLMs in *mtm*-depleted abdomens (Figure 1D′–1E; Figure S1D′–S1E). The remaining *mtm*-depleted myofibers were frequently detached and seen as rounded-up balls or as elongated fibers with one completely detached end (Figure 1D′, 1F; Figure S1D′, S1F), never observed in controls.

To explore the developmental requirement for an *mtm* muscle function, we first characterized myofibers using timelapse microscopy in intact animals. With *mtm* depletion, GFP-labeled IOMs were properly maintained during early pupal stages, when other larval muscles undergo developmentally regulated cell death (Figure 1A,1G–1G′, 2 days after pupal formation, APF). The *mtm*-depleted IOMs subsequently underwent normal myofiber thinning (3d APF) and rethickening (4d APF), indicative of developmental turnover and rebuilding of the contractile myofibrils [25]. While no detachment was observed in control animals ($n = 19$), IOM detachment occurred during remodeling in late pupal stages with *mtm* knockdown ($n = 15$) (Figure 1G′, 4d APF). Thus, *mtm* is not essential for IOM formation or survival, but is important for muscle attachments and maintenance upon remodeling.

To address whether *mtm* plays a role in other muscles, we examined different developmental stages and myofiber types. Although adult somatic muscles appeared to form normally with muscle-specific *mtm* knockdown (Figure 1D′ and not shown), $100.0 \pm 0.0\%$ of the viable adult flies were flightless (versus $22.2 \pm 5.4\%$ control; $n = 10$, ≥ 124 flies). Visceral muscles that normally migrate to ensheath the testis [26] were present but also disrupted with *mtm* muscle-depletion (Figure S1G–S1G′, 24B-GAL4). Taken together, *mtm* function appears dispensable for myogenesis, but is broadly required in both somatic and visceral muscles for myofiber remodeling, maintenance and function.

Mtm disruption models centronuclear myopathy, including T-tubule disorganization

Pathological hallmarks of XLMTM are small, rounded myofibers with nuclei displacement and disorganization of the perinuclear compartment [8]. In wildtype IOMs, myofibrils are normally tightly packed around centrally aligned nuclei following myofiber remodeling [25] (Figure 1H). In contrast, in *mtm*-depleted IOMs, central myofibrils were misaligned or absent around a normal number of centrally-displaced nuclei (2.1-fold increased nuclei distance from midline; Figure 1H′–1J). The nuclei were otherwise normal in size and morphology (Figure S2A–S2A′) and pharate adult IOMs were impermeable to propidium iodide staining (Figure S2B–S2C′), while ultrastructural analysis confirmed normal mitochondrial integrity (Figure S2D–S2D′), all indicating viability of *mtm*-depleted IOM cells. The peripheral

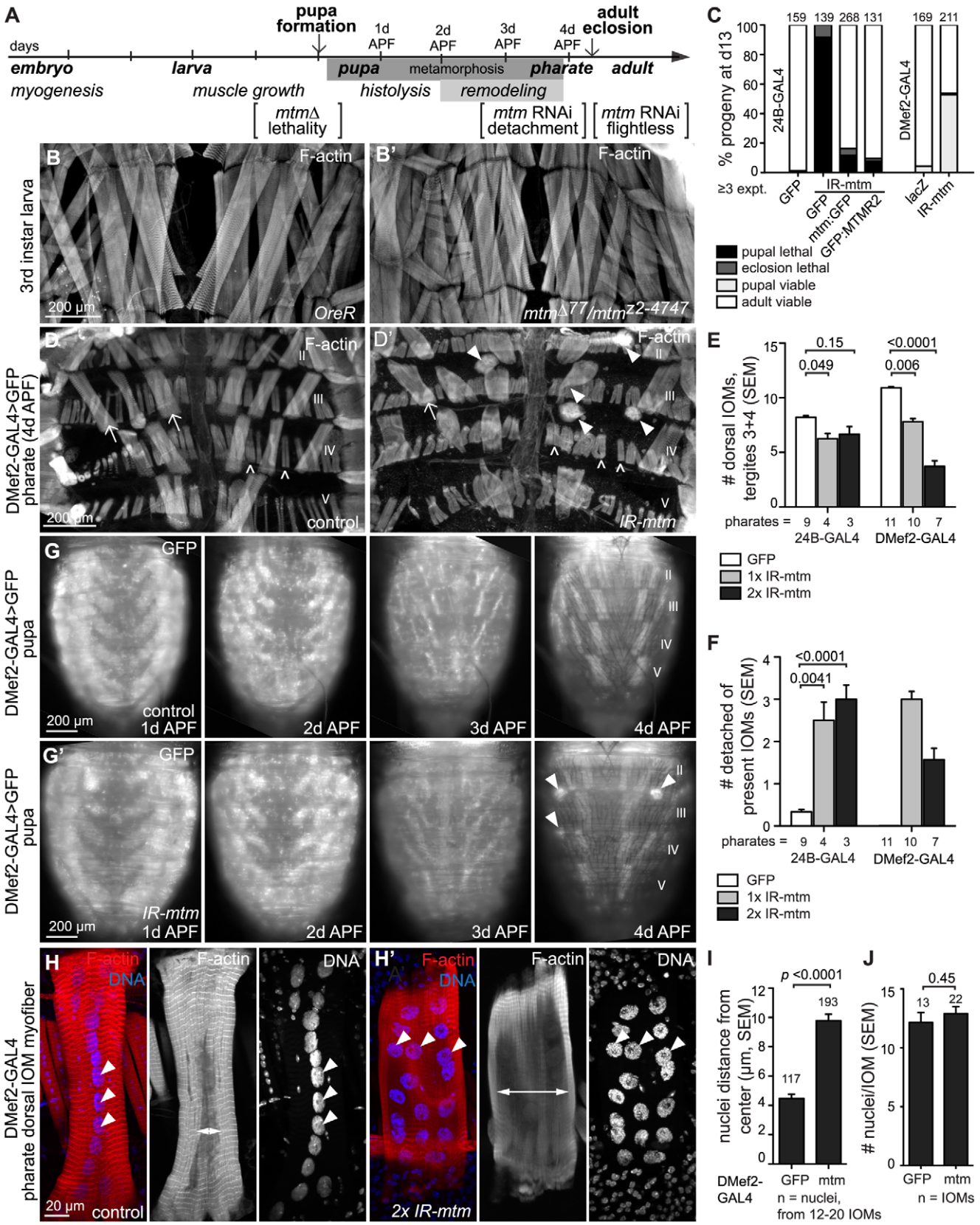

Figure 1. Mtm depletion leads to myofiber detachment and morphological defects common with human myotubular myopathy. (A) Timeline of fly and muscle development, indicating stages of *mtm* requirements; days after puparium formation (APF). (B–B′) Normal body wall muscles in *OreR* and $mtm^{\Delta 77}/mtm^{z2\text{-}4747}$ third instar larvae. F-actin. (C) Percent viable and lethal progeny 13 days after egg lays with 24B-GAL4 and DMef2-GAL4 muscle-targeted *mtm* RNAi. (D–D′) Pharate dorsal abdominal muscles F-actin. Large IOMs (arrows) and smaller adult muscles (open

arrowheads) span tergites (numerals). (D′) Detached IOMs (arrowheads) seen with *mtm* RNAi. (E–F) IOMs in filleted abdomens with 24B-GAL4 or DMef2-GAL4 expression of 1 or 2 copies of *mtm* RNAi hairpins. (E) Number IOMs present in tergites 3 and 4, including detached but present IOMs. (F) Number of present, visibly detached IOMs. (G–G′) Timelapse microscopy of GFP in IOMs imaged in same animals 1, 2, 3 and 4 days APF. (G′) With *mtm* RNAi, normal IOM formation (1d APF), survival upon histolysis of non-persistent muscles (2d APF), myofiber thinning (3d APF) and rethickening (4d APF) preceded detachment (4d APF, arrowheads). (H–H′) Individual IOMs. F-actin, red; DNA, blue. Projections, merged and nuclei images; central z-sections, F-actin. (H) Contractile myofibrils are normally tightly packed (double arrow) around linear aligned nuclei (arrowheads). (H′) With *mtm* RNAi, intact peripheral myofibrils surround expanded central area (double arrow) with unaligned nuclei (arrowheads). (I) Distance (μm) of nuclei from IOM midline. (J) Number nuclei per IOM. Scale bar 200 μm, except H–H′ 20 μm.
doi:10.1371/journal.pgen.1001295.g001

myofibrils appeared normal (Figure S2E–S2H), suggesting that *mtm* is unlikely to function directly in sarcomere assembly.

We also found that transverse (T)-tubules were disrupted in *mtm*-depleted myofibers, consistent with defects recently described in vertebrate XLMTM [14,27]. T-tubules are an extensive membrane network, continuous with the sarcolemma, which mediates excitation-contraction coupling throughout the myofiber interior. Although critical for force-generating contractions, there is little understanding of T-tubule biogenesis and structural regulation. We found that both the Amphiphysin (Amph) BAR-domain protein and Dlg1 membrane-associated guanylate kinase scaffold protein localize to T-tubules in wildtype abdominal myofibers (Figure S3A, S3B, S3C), as in flight muscles [28]. In *mtm*-depleted IOMs, although longitudinal elements of T-tubule membranes were present, lack of Amph and Dlg indicated that transversal membranes were specifically disorganized or absent (Figure S3A′, S3B′; 9.5% control versus 96.3% *mtm* RNAi with transversal membranes in <half of IOM; $n \geq 21$). These conclusions were confirmed by transmission electron microscopy (Figure S3D–S3D′). Altogether, the conserved mutant phenotypes and timing of onset suggests that *mtm*-depleted muscles in flies model hallmarks of XLMTM.

Mtm is required for βPS-integrin trafficking for adhesions in muscle and wing

Given the muscle detachment and myofibril misalignment observed in *mtm* mutant myofibers, we considered a possible defect in IACs at MTJs and costameres (Figure 2A–2C). We found that βPS-integrin, the single *D. melanogaster* β-integrin subunit encoded by *mys* (GenBank NM_080054), was dramatically mislocalized in *mtm*-depleted muscles (Figure 2B′). In contrast to wildtype muscle, βPS-integrin was absent at the ends of detached myofibers (Figure 2B″) and from costameres (Figure 2C′), consistent with detachment due to disruption of integrin adhesions. Although an intracellular pool of βPS-integrin protein was detected as small punctae within wildtype myofibers (Figure 2D), upon *mtm* knockdown, βPS-integrin became enriched along abnormal vacuolar inclusions within the myofiber center (Figure 2D′). Ultrastructural analyses revealed large, lucent membrane-bound compartments within the central regions of the *mtm*-depleted but not control myofibers (Figure 2E–2E″). Other proteins of the integrin adhesion complex, αPS2-integrin and Talin, were both detected at MTJs but not at the inclusions, suggesting βPS-integrin as a primary target of *mtm* function (Figure S4A–S4B′).

To address the possible relationship between the appearance of membrane inclusions and muscle detachment, we examined βPS-integrin localization at earlier developmental stages. In *mtm* null or RNAi depleted larval muscles, normal integrin localization was detected at myofiber attachments, without any βPS-integrin-containing central inclusions (Figure S4C, S4C′). This indicates that appearance of inclusions coincides with detachment, and that *mtm* function is not needed for initial IAC formation. Although detected at the larval myofiber surface, βPS-integrin was not organized into uniform striations in either wildtype or mutant myofibers, as compared to the costameres observed in wildtype pharate adult IOMs. To address whether *mtm* function affects integrin trafficking prior to myofiber remodeling and detachment, we performed FRAP analysis of βPS-integrin:YFP along MTJs in intact larvae [6]. The mobile fraction of βPS-integrin:YFP was significantly increased in *mtm* mutant larval muscles (Figure 2F), indicating that *mtm* is required to stabilize sarcolemmal βPS-integrin localization, preceding myofiber remodeling.

To explore a basis for the sensitivity to *mtm* loss of function in pupal stages, we investigated integrin localization during IOM remodeling in metamorphosis. In wildtype myofibers at 2–3 days after pupal formation (APF), we discovered that there was a normal loss of integrin from the cell surface, along with detectable presence of integrin-marked inclusions (Figure 2G–2H). By 4 days APF, integrin was again predominantly absent in the myofiber center, with reappearance at costameres. This result reveals a normal redistribution of integrin that occurs with IOM remodeling, and suggests a distinct requirement for myofiber integrin regulation in pupal stages. To test a temporal requirement for *mtm* function specifically in pupal stages, we performed temperature shift experiments to induce conditional *mtm* knockdown. Due to the temperature sensitivity of the GAL4 transcription factor, flies with muscle-targeted *mtm* hairpin expression maintained normal myofiber attachments when raised continuously at 18°C with low GAL4 activity (Figure S4D). However, when flies were shifted during metamorphosis to 29°C for 1–2 days with increased GAL4 activity, the pharate adults then exhibited myofiber detachment (Figure S4D′–S4E, 0% versus 71% *mtm* pharates, respectively). Similarly, flies also carrying the temperature sensitive $GAL80^{ts}$, an inhibitor of GAL4, raised continuously at 18°C did not exhibit integrin-containing inclusions (Figure S4F, 0%). In contrast, flies shifted to 29°C for 3 days (with shorter metamorphosis at higher temperatures), exhibited myofibers with integrin-containing inclusions (Figure S4F′–S4G, 58%). These results indicate a requirement for *mtm* function in pupal stages that is important for integrin localization at the cell surface following myofiber remodeling, and further supports a primary role for *mtm* in integrin trafficking.

The requirement for *mtm* function in myofiber remodeling during development raised the question whether there is a similar *mtm* requirement during cellular remodeling that may occur with ongoing adult muscle use, repair or ageing. We investigated integrin localization in adult abdominal myofibers, which are derived from a different developmental program from the persistent larval muscles. The long, thin adult ventral abdominal muscles, called lateral transversal muscles, normally exhibit a striated pattern of intense integrin localization at repeating costameres (Figure 2I). In contrast, integrin deviated from this pattern with a diffuse distribution in portions of *mtm*-depleted myofibers in both six and ten day old adult flies (Figure 2I′). This result points to an important role for *mtm* in the maintenance of integrin adhesions with ongoing muscle use in adult flies.

To test whether *mtm* function has a specific role for integrin localization in broader developmental contexts, we assayed function of integrin-mediated adhesions in the epithelial bilayer of the developing fly wing [1]. The low frequency of wing blisters

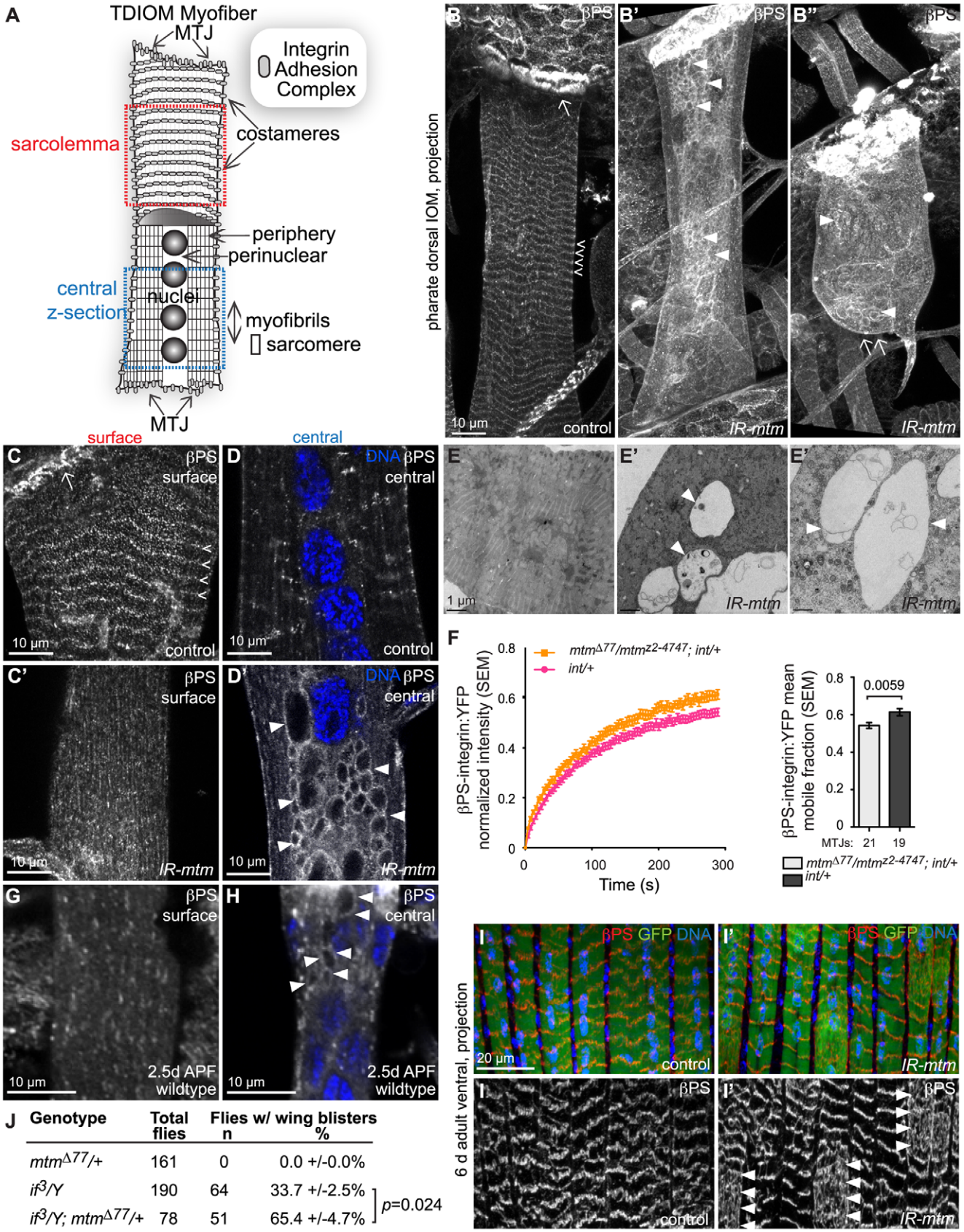

J Genotype	Total flies	Flies w/ wing blisters n	%
$mtm^{\Delta 77}/+$	161	0	0.0 +/-0.0%
if^{3}/Y	190	64	33.7 +/-2.5%
$if^{3}/Y; mtm^{\Delta 77}/+$	78	51	65.4 +/-4.7%

p=0.024

Figure 2. Mtm is required for βPS-integrin flux from intracellular compartments and localization at sarcolemmal adhesions. (A) Schematic of individual pharate IOM and regions imaged. MTJ, myotendinous junction. (B–B″) βPS-integrin in IOM z-projections. (B) βPS-integrin at MTJs (arrow) and costameres (open arrowheads) in control. (B′–B″) With *mtm* RNAi, βPS-integrin was absent from detached ends (B″, arrow) and

costameres, and detected on abnormal inclusions (arrowheads). (C–C′) IOM sarcolemma highlighting βPS-integrin at costameres in control (C, open arrowheads), absent with *mtm* RNAi (C′). (D–D′) IOM central z-sections revealing βPS-integrin punctae in control (D), and accumulation on abnormal inclusions with *mtm* RNAi (D′, arrowheads). DNA, blue. (E–E′) Transmission electron microscopy of IOM cross-sections, showing densely packed central regions in control (E) and large lucent membrane compartments with *mtm* RNAi (E′, arrowheads). (F) Averaged FRAP recovery curves and mean mobile fraction for larval βPS-integrin:YFP (*int*/+) in wildtype background (pink) and trans-heterozygous null $mtm^{\Delta 77}/mtm^{z2\text{-}4747}$ (orange). (G) Little to no βPS-integrin present at the sarcolemma in wildtype pupal IOM, 2.5 days APF. (H) βPS-integrin on central inclusions (arrowheads) detected in wildtype pupal IOM, 2.5 days APF. DNA, blue. (I–I′) βPS-integrin (red, and single channel below) at costameres in z-projections of adult abdominal lateral transversal muscles (I), and sporadically absent from costameres and dispersed in regions of myofibers with *mtm* RNAi (I′) in 6 day old adult flies. GFP, green; DNA, blue. *DMef2-GAL4*. (J) Heterozygous $mtm^{\Delta 77}$/+ enhanced frequency of adult wing blisters in hemizygous if^3/Y flies. Scale bars 10 μm, except E–E′ 1 μm.
doi:10.1371/journal.pgen.1001295.g002

resulting from a hypomorphic allele of αPS2-integrin, if^3 [29], was dominantly enhanced when in combination with heterozygous *mtm* null alleles with reduced function (Figure 2J), similar to interactions seen with components known to be required for integrin adhesions [30]. The interaction in two different tissues suggests a specific and fundamental role for *mtm* in maintenance of integrin-mediated attachments.

Integrin adhesions and T-tubules have independent requirements for Mtm function

The disruption in *mtm* mutants of both IACs and T-tubules, and their normal proximity along the sarcolemma, raised the question whether a structural or functional relationship between the two compartments normally exists or is relevant to the abnormal membrane inclusions (Figure 3A). Moreover, in *mtm*-depleted myofibers, we noted that Dlg, similar to βPS-integrin, appeared along abnormal central inclusions (Figure 3B, 3B′). To characterize the membrane identity of the inclusions, we first tested whether βPS-integrin and Dlg or Amph co-localized, either in normal or *mtm* mutant muscles. In wildtype myofibers, Dlg and Amph were not detected at IACs. However, internal βPS-integrin frequently co-localized with Dlg (Figure 3C) and occasionally with Amph (Figure S5A, S5B, S5C) along apparent longitudinal elements of T-tubules. Upon *mtm* depletion, βPS-integrin extensively co-localized with Dlg and Amph on longitudinal T-tubules (Figure S5A, S5B′) and along the central inclusions (Figure 3C′, Figure S5B″), suggesting accumulation of a possible common precursor membrane or trafficking compartment in *mtm*-depleted muscles.

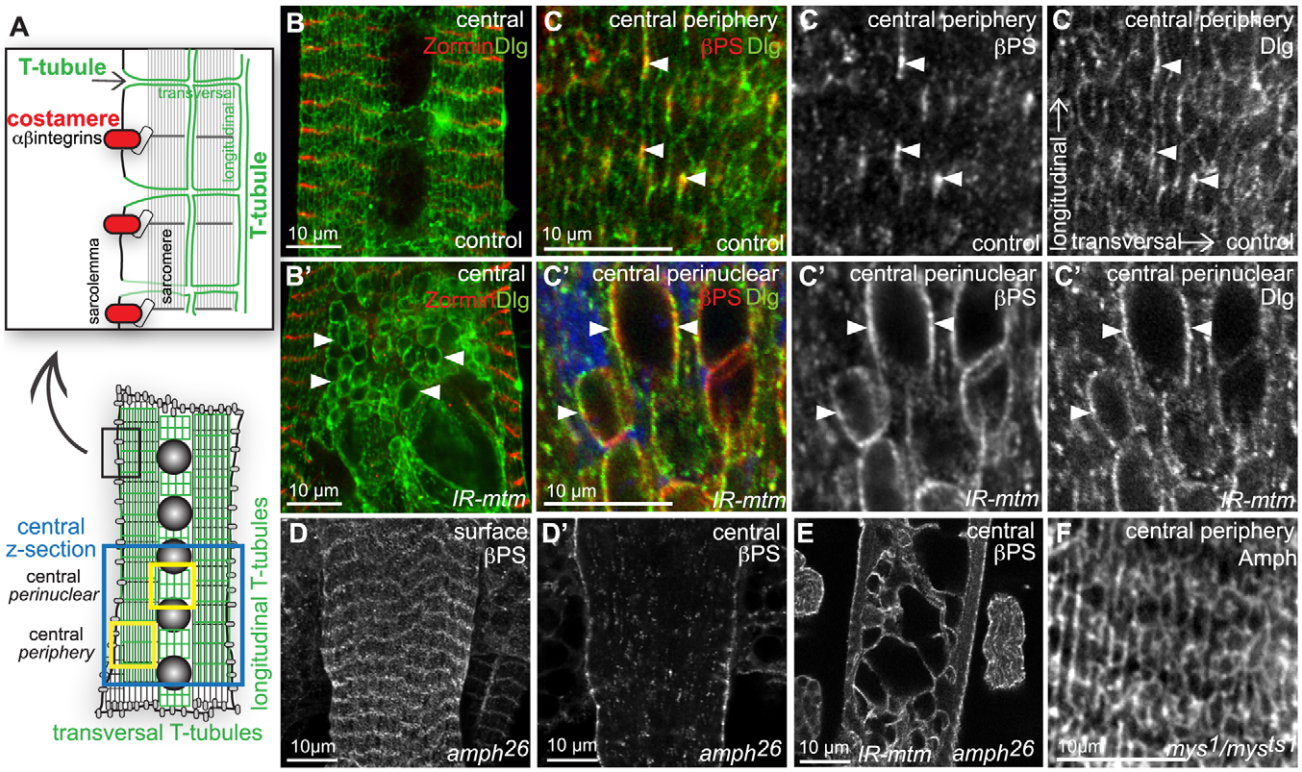

Figure 3. Integrin adhesions are independent of T-tubules, but share an *mtm* function for maintained organization. (A) IOM longitudinal section schematic of alternating sarcolemmal structures: T-tubule membranes (green) marked by Amph and Dlg; costameres (red) with IACs linked to Z-lines of peripheral myofibrils; z-section images from central, central periphery or central perinuclear regions, as shown. (B–B′) Dlg, green; Zormin, red. Dlg detected continuously on longitudinal and transversal T-tubules in control (B), but only on longitudinal tubules and on central inclusions with *mtm* RNAi (B′, arrowheads). (C–C′) βPS-integrin (red) and dlg1:GFP (green) partially co-localized at longitudinal T-tubules in control (C, open arrowheads), and on abnormal central inclusions with *mtm* RNAi (C′, arrowheads). Single channels, right. (D) Normal βPS-integrin localization at costameres and (D′) internal punctae in $amph^{26}$ mutants that lack T-tubules. (E) Persistent βPS-integrin-inclusions with *mtm* RNAi in $amph^{26}$ mutant. $amph^{26}$, *UAS-IR-mtm*$^{3.1}$/$amph^{26}$; *DMef2-GAL4*/+. (F) Normal transverse tubule formation and Amph localization in mys^1/mys^{ts1} mutants reared at non-permissive temperature, with reduced βPS-integrin function. Scale bars 10 μm.
doi:10.1371/journal.pgen.1001295.g003

We next considered whether there is functional co-dependence between integrin adhesions and T-tubules. In *amph*^{26} null mutants that lack T-tubules in IOMs (Figure S5D), as in adult flight muscles [28], we observed normal muscle attachments, normal βPS-integrin localization to costameres, and no βPS-integrin- or Dlg-inclusions (Figure 3D–3D′). This suggests that T-tubules are not required for βPS-integrin trafficking in the formation or maintenance of IACs, and that the inclusion defects in *mtm* mutants do not reflect a general consequence of failed T-tubule formation. Furthermore, we found βPS-integrin mislocalized to internal membrane inclusions upon *mtm* depletion in *amph*^{26} null mutants (Figure 3E), signifying that the abnormal inclusions are independent of transverse tubule membrane and possible misregulation of *amph* function. Conversely, transverse tubules were present normally in abdominal muscles with hypomorphic *mys* conditions that were pharate lethal (Figure 3F), suggesting that T-tubule organization does not require normal levels of βPS-integrin protein or IACs. The dramatic defects in both IACs and T-tubule organization upon *mtm* depletion therefore appear to reflect a requirement for two independent *mtm* functions.

PI(3)P role in Mtm-dependent muscle compartmentalization

The disrupted βPS-integrin localization together with the enlarged membrane inclusions suggested defective membrane trafficking in *mtm* mutant myofibers. Characterization of the central inclusions could point to a specific compartment or trafficking step that normally requires Mtm phosphatase activity in muscle remodeling. The inclusions did not noticeably contain markers of endoplasmic reticulum, the trans-Golgi network or autophagosomes (Figure S5E–S5E′ KDEL; Figure S5F–S5F′ PH-FAPP1; Figure S5G–S5G′ Atg8). In contrast, the majority of inclusions were decorated by the endosome-lysosomal marker, GFP:LAMP (Figure 4A–4A″). The inclusions were frequently colocalized with an indicator of early

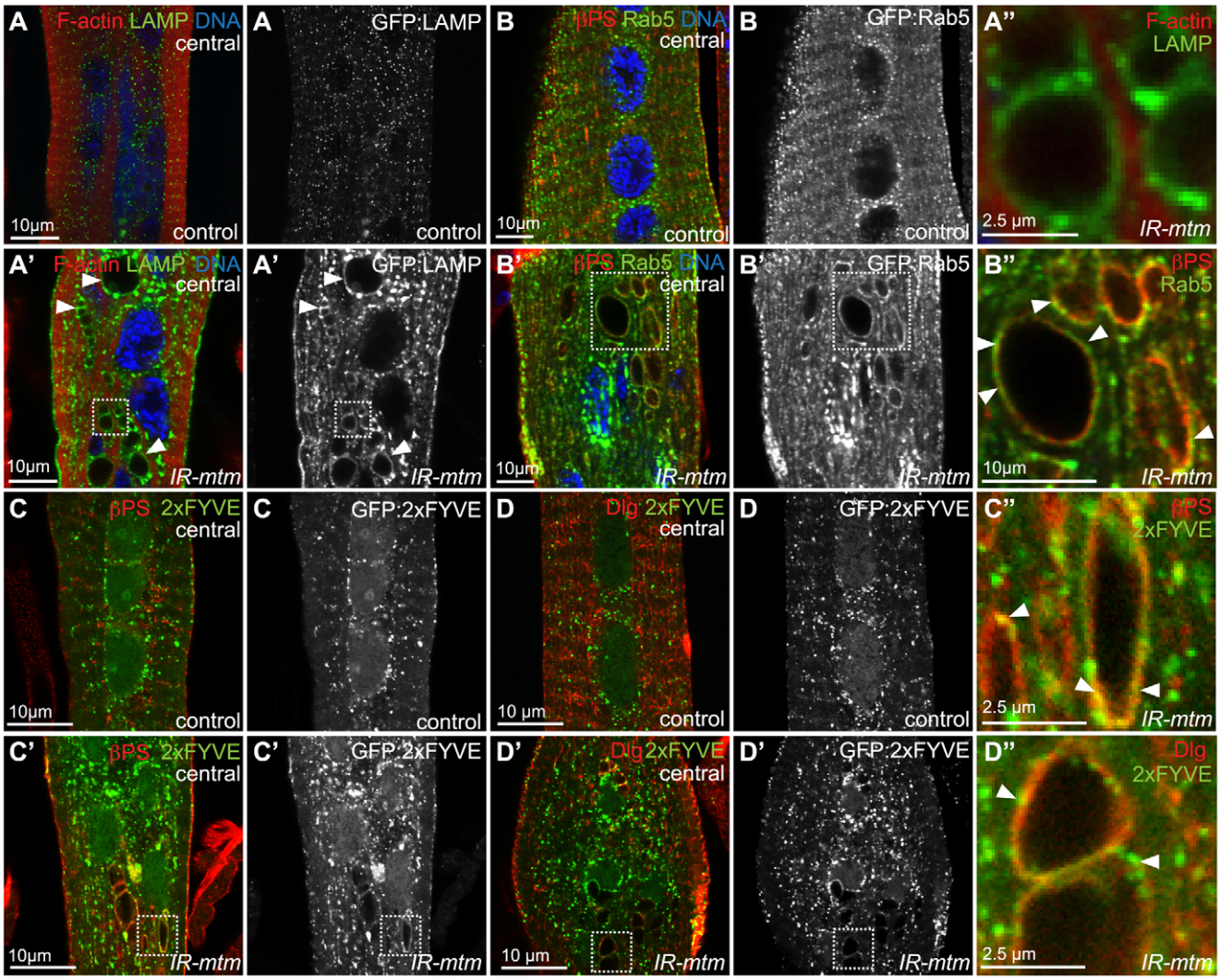

Figure 4. Mtm depletion disrupts integrin trafficking at endosomal compartments. (A–A″) GFP:LAMP (green, and single channels) found as punctae throughout IOM controls (A) and localized to inclusions with *mtm* RNAi (A′, arrowheads; A″). F-actin, red; DNA, blue. (B) GFP:Rab5 (green, and single channels) found as punctae with normally little overlap with βPS-integrin (red) throughout IOM controls. (B′–B″) Rab5 partially co-localized with βPS-integrin on inclusions and accumulated at the plasma membrane and perinuclear with *mtm* RNAi. DNA, blue. (C–C″) PI(3)P detected by GFP:2xFYVE (green, and single channels) and βPS-integrin (red) exhibited little overlap in control (C), but co-localized on inclusions with *mtm* RNAi (C′–C″, arrowheads). (D–D″) PI(3)P detected by GFP:2xFYVE (green) and Dlg (red) exhibited little overlap in control (D), but co-localized on inclusions with *mtm* RNAi (D′–D″, arrowheads). Scale bars 10 µm, except zooms A″, C″, D″ 2.5 µm.
doi:10.1371/journal.pgen.1001295.g004

endosomes, GFP:Rab5 (Figure 4B–4B″), and infrequently by the Rab5 effector, Rbsn5 (Figure S5H–S5H′), but not an indicator of late endosome identity, GFP:Rab7 (Figure S5I–S5I′). Together, these results suggest a relationship between the inclusions and early endocytic traffic, and that *mtm* depletion disrupts endocytic traffic.

PI(3)P is normally enriched at endosomal membranes. We have recently shown that the normal Mtm PI(3)P phosphatase activity promotes membrane efflux, effecting both endosomal homeostasis and cortical remodeling in macrophages [18]. We therefore explored PI(3)P distribution in muscle with respect to integrin adhesion and T-tubule compartments. In wildtype animals, muscle expression of the PI(3)P biosensor, GFP:2xFYVE, was detected along the sarcolemma and localized to punctae distributed throughout abdominal myofibers, with the greatest concentration in the perinuclear area without obvious overlap with βPS-integrin (Figure 4C) or Dlg (Figure 4D). Upon *mtm*-depletion, enlarged and more erratically positioned PI(3)P-containing compartments were detected (Figure 4C′, 4D′). In addition, GFP:2xFYVE co-localized with βPS-integrin (Figure 4C″) and with Dlg (Figure 4D″) along the abnormal inclusions in *mtm*-depleted myofibers, suggesting a possible role for Mtm phosphatase activity in PI(3)P turnover involved in integrin trafficking.

Pi3KC2 suppresses Mtm-related defects in βPS-integrin localization and muscle maintenance

To test if PI(3)P regulation is involved in *mtm* muscle functions, we investigated the contribution of Class II and III Pi3-kinases (*Pi3K68D* and *Vps34*, respectively), known to synthesize PI(3)P, to abdominal muscle maintenance. Muscle-targeted knockdown of *Pi3K68D* or expression of dominant negative kinase-dead *Vps34-KD* did not individually disrupt eclosion or animal viability. However, *Pi3K68D* depletion in combination with *mtm* RNAi was able to rescue the lethality and delayed development; in contrast, *Vps34-KD* expression enhanced lethality in combination with *mtm* depletion (Figure S6A, S6B). Neither *Pi3K68D* nor *Vps34* knockdown rescued the loss of T-tubules with *mtm*-depletion (Figure S6C), and accordingly adult flies remained flightless (Figure S6D). These results indicate separable *Pi3K68D*-independent and dependent *mtm* muscle functions required for normal T-tubules and viability, respectively.

A similar functional relationship was seen between *Pi3K68D* and *mtm* for roles related to integrin adhesions, as with viability. Importantly, *Pi3K68D*, but not *Vps34*, depletion rescued muscle detachment (Figure 5A, 5B) and loss of βPS-integrin localization at costameres (Figure 5C, 5C′, 5D) that occurs with loss of *mtm* function. Consistent with rescue of the IACs, co-depletion of *mtm* and *Pi3K68D*, and not *Vps34*, also eliminated the βPS-integrin- and Dlg-containing membrane inclusions (Figure 5E, 5E′, 5F, Figure S6E), indicating a functional relationship between the abnormal central inclusions and IACs at the sarcolemma. The testis visceral muscle function was also restored to normal with *Pi3K68D* and *mtm* co-depletion, implicating turnover of integrin-mediated adhesions in the gonadal muscle. Altogether, these results signify that *Pi3K68D* function mediates *mtm* RNAi mutant defects in maintenance of IACs, and suggest that Pi3K68D may synthesize a PI(3)P subpool co-regulated by Mtm important for integrin trafficking and localization.

Interestingly, muscle-targeted disruption of *Vps34* shared with *mtm* depletion a similar staged semi-lethality (Figure S6A), IOM detachment (Figure 5A′, 5B) and loss of βPS-integrin at costameres (Figure 5C″, 5D), however, without inducing abnormal inclusions (Figure 5E″, 5F, Figure S6E). This points to possible shared or sequential roles for Vps34 and Mtm in phosphoinositide-mediated steps in IAC maintenance, distinct from trafficking points that involve antagonistic Pi3K68D and Mtm co-regulation. Vps34 is broadly attributed with roles in PI(3)P-regulated endocytosis and autophagy. We found that inhibition of autophagy upon depletion of the central regulator, *Atg1*, phenocopied the *Vps34* integrin defects (Figure S6F, S6G, S6H), indicating an important role for autophagy in IOM remodeling. We tested whether the phenotypes associated with m*tm* phosphatase depletion are a result of increased PI(3)P-mediated autophagy. The myofiber detachment and integrin localization defects, including integrin-containing inclusions, persisted with co-depletion of *Atg1* and *mtm* (Figure S6F′, S6G′, S6H′), indicating that autophagy is not responsible for the integrin-related defects upon *mtm* depletion.

Integrin is mislocalized in human myofibers with XLMTM myopathy

Given shared defects observed in *mtm*- and *MTM1*-disrupted myofibers in flies and human XLMTM, respectively (Figure 1H′, Figure S3A′–S3D′), we asked whether an *mtm* function required for integrin adhesions is also shared with *MTM1* in human muscle. β1-integrin, the major β-integrin isoform found in vertebrate muscle, was detected along the myofiber sarcolemma in cross-sections of skeletal muscle from control subjects, as expected (Figure 6A). In contrast, β1-integrin localized throughout the perinuclear compartment of centronucleated myofibers in muscle from neonates with XLMTM (Figure 6B). The Dystroglycan adhesion complex (DAC) is a second complex localized to MTJs and costameres with key roles in muscle attachments, and mutations of DAC components are frequently associated with muscular dystrophy. Unlike integrin, the dystroglycan transmembrane protein exhibited only the expected peripheral staining along the sarcolemma in both control and XLMTM myofibers, without any abnormal centronuclear localization or inclusion (Figure 6C–6D). These results show that *MTM1* is specifically required for normal β1-integrin localization in human myofibers, and suggests that disruption of integrin trafficking and adhesion complex function is important in XLMTM.

Discussion

We found that *mtm* regulates integrin adhesions in muscle and in the developing wing, and that integrin localization was disrupted in human XLMTM, pointing to a central role for Mtm/MTM1 in a trafficking pathway important for localization of β-integrin at the plasma membrane. It is well-established that integrin turnover contributes to cell motility, whereby targeted integrin recycling and reassembly of localized adhesions mediate polarized matrix attachments and signaling responses [4]. Our results reveal that regulated integrin turnover is also important for integrin adhesions in non-motile myofibers, after the establishment of attachments. Importantly, *mtm* disruption uncovered a demand for βPS-integrin trafficking in the maintenance of adhesions both at MTJs as well as at costameres, a less-understood adhesion site with putative roles in muscle integrity, mechanotransduction, and myofibril assembly [31,32]. Although integrin was destabilized at larval MTJs in *mtm* mutants, the most severe consequences occurred later with specific loss of pupal or adult *mtm* function during developmental myofiber remodeling or adult muscle use, respectively. This is consistent with costamere sensitivity to integrin depletion in adult muscle [33] and the possibility that *mtm* similarly regulates integrin turnover with myofiber remodeling that occurs both in development and with demands in adult muscle growth, repair and aging.

In fly macrophages, Class II *Pi3K68D* and *mtm* co-depletion could revert both an imbalance in PI(3)P and defects in cortical

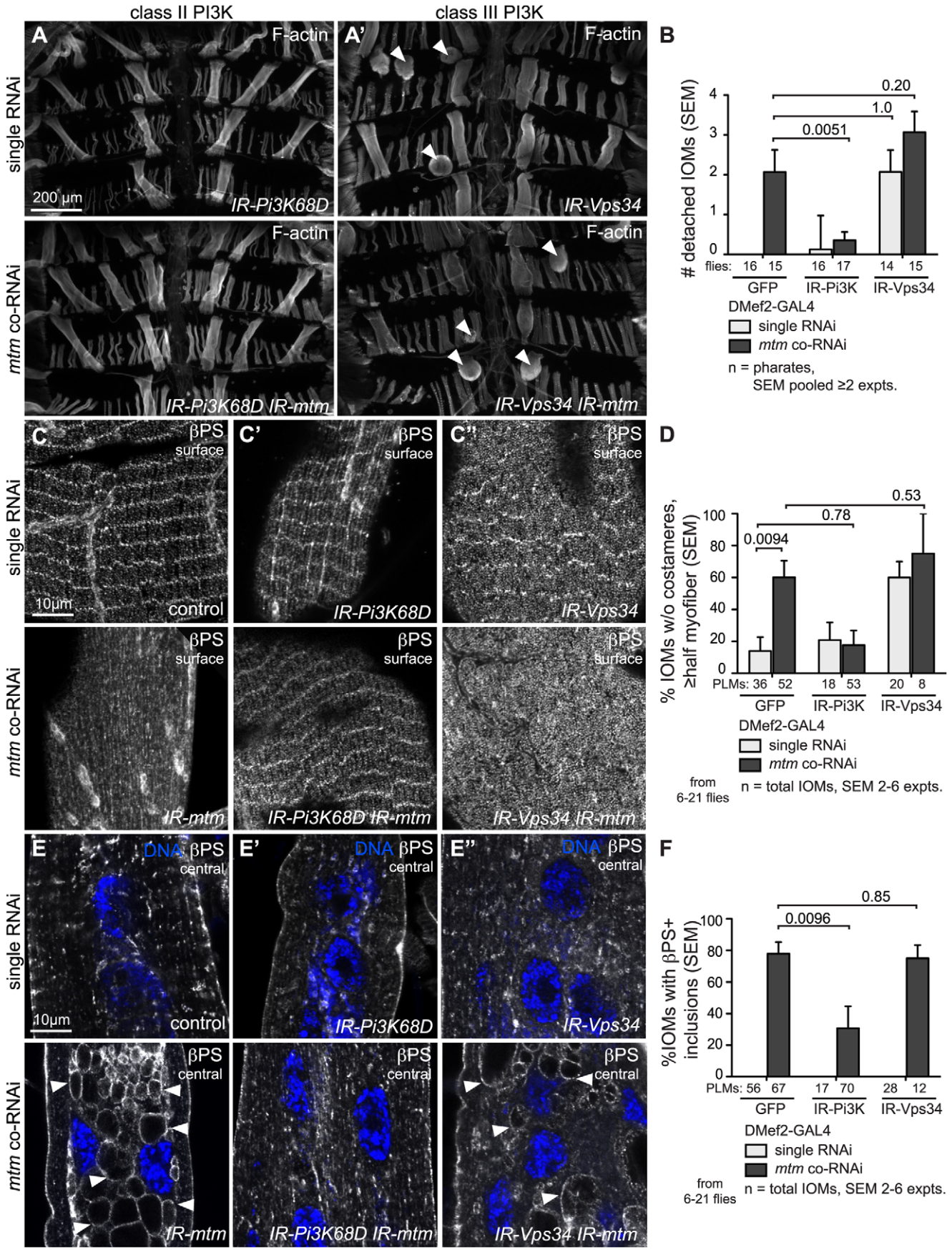
class II PI3K
class III PI3K
A
F-actin
A'
F-actin
single RNAi
200 µm
IR-Pi3K68D
IR-Vps34
mtm co-RNAi
F-actin
F-actin
IR-Pi3K68D IR-mtm
IR-Vps34 IR-mtm
B
detached IOMs (SEM)
0.20
1.0
0.0051
flies: 16 15 16 17 14 15
GFP
IR-Pi3K
IR-Vps34
DMef2-GAL4
single RNAi
mtm co-RNAi
n = pharates,
SEM pooled ≥2 expts.
C
βPS
surface
C'
βPS
surface
C''
βPS
surface
single RNAi
10µm
control
IR-Pi3K68D
IR-Vps34
mtm co-RNAi
βPS
surface
βPS
surface
βPS
surface
IR-mtm
IR-Pi3K68D IR-mtm
IR-Vps34 IR-mtm
D
% IOMs w/o costameres, ≥half myofiber (SEM)
0.53
0.78
0.0094
PLMs: 36 52 18 53 20 8
GFP
IR-Pi3K
IR-Vps34
DMef2-GAL4
single RNAi
mtm co-RNAi
from 6-21 flies
n = total IOMs, SEM 2-6 expts.
E
DNA βPS
central
E'
DNA βPS
central
E''
DNA βPS
central
single RNAi
10µm
control
IR-Pi3K68D
IR-Vps34
mtm co-RNAi
βPS
central
βPS
central
βPS
central
IR-mtm
IR-Pi3K68D IR-mtm
IR-Vps34 IR-mtm
F
%IOMs with βPS+ inclusions (SEM)
0.85
0.0096
PLMs: 56 67 17 70 28 12
GFP
IR-Pi3K
IR-Vps34
DMef2-GAL4
single RNAi
mtm co-RNAi
from 6-21 flies
n = total IOMs, SEM 2-6 expts.

Figure 5. Class II and Class III PI3-kinases affect *mtm*-dependent integrin adhesions differently. (A–A′) Pharate abdominal muscles, F-actin. (A) *IR-Pi3K68D* and (A′) *IR-Vps34* single RNAi (top) and *mtm* co-RNAi (bottom). Arrowheads, detached IOMs. (B) Number of visibly detached IOMs. (C, C′, C″) Sarcolemmal βPS-integrin detected at costameres; (C) control, (C′) *IR-Pi3K68D* and (C″) *IR-Vps34* in single RNAi (top) and *mtm* co-RNAi (bottom). Only *Pi3K68D*, *mtm* co-RNAi restored βPS-integrin at costameres. (D) Percentage IOMs that lack costameres ≥half of myofiber surface. (E, E′, E″) βPS-integrin central *z*-sections; (E) control, (E′) *IR-Pi3K68D* and (E″) *IR-Vps34* single RNAi (top) and *mtm* co-RNAi (bottom). Only *Pi3K68D*, *mtm* co-RNAi reverted abnormal βPS-integrin-inclusions. (F) Percentage IOMs with βPS-integrin on inclusions. (B,D,F) IOMs in single RNAi (light bars) and *mtm* co-RNAi (dark bars) conditions. Scale bars 10 μm, except A–A′ 200 μm.
doi:10.1371/journal.pgen.1001295.g005

remodeling that impaired macrophage shape and *in vivo* immune cell distribution [18]. Here, we found *Pi3K68D* disruption is also a specific and potent suppressor of integrin adhesion defects in *mtm*-depleted muscle. Despite distinct macrophage and myofiber morphology and function, a shared requirement for a PI3KC2/Mtm pathway highlights common functions during cellular remodeling.

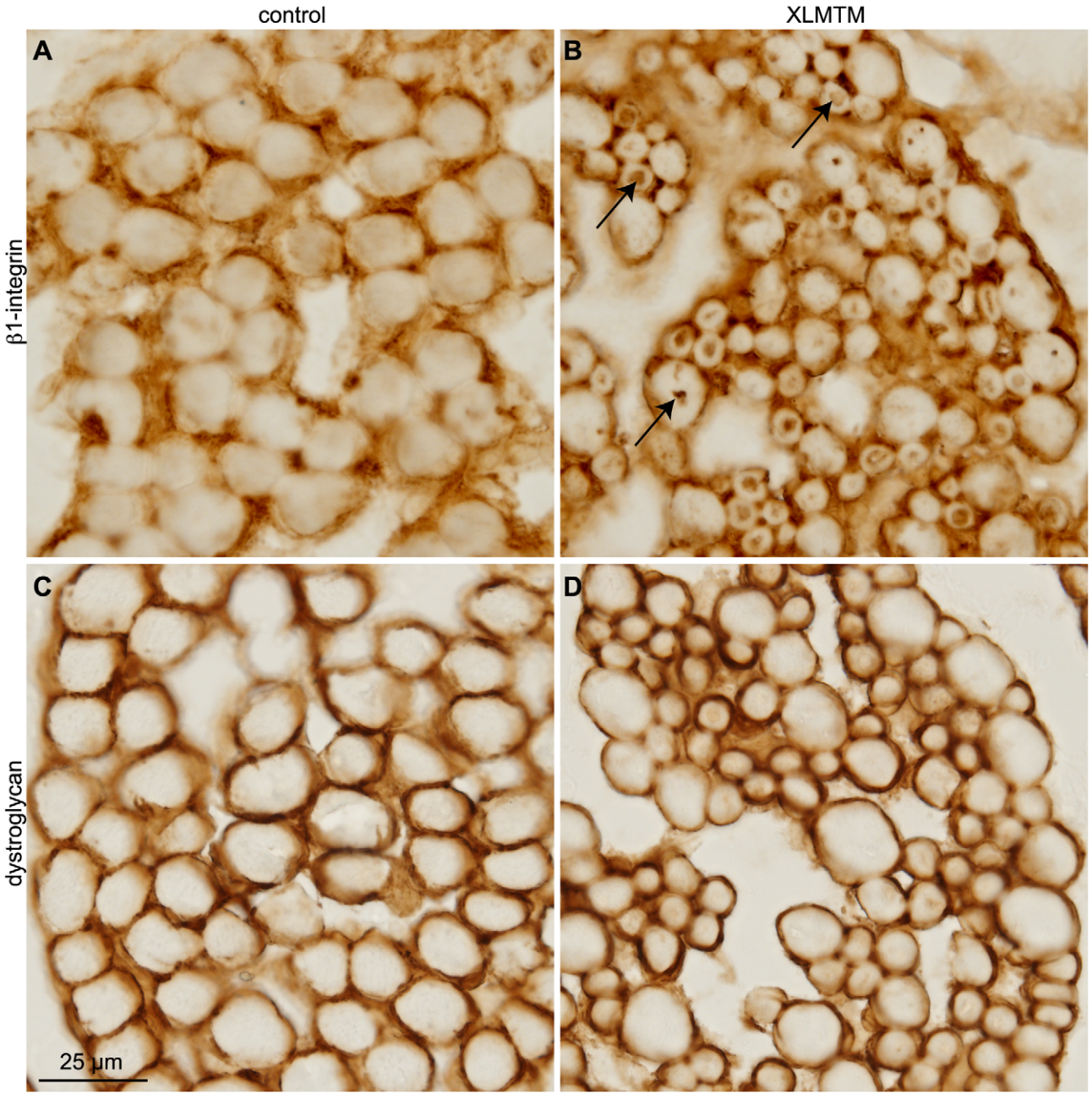

Figure 6. β1-integrin is mislocalized to perinuclear inclusions in XLMTM myopathy. Cryosections from XLMTM (n = 3) and age-matched control human muscle biopsies were immunostained either with anti-β-dystroglycan or with anti-β1D-integrin. (A–B) β1D-integrin was found only along the sarcolemma in control muscle (A), but was mislocalized to the perinuclear compartment in XLMTM fibers (B, arrows). (C–D) In contrast, Dystroglycan was found normally distributed along the sarcolemma membrane in both control (C) and XLMTM (D) muscle. Scale bar, 25 μm.
doi:10.1371/journal.pgen.1001295.g006

Loss of Mtm phosphatase activity could be considered a gain of function condition, analogous to ectopic kinase activity, leading to inappropriate phosphoinositide accumulation. In line with this, either *mtm* depletion (this study) or *Pi3K68D* overexpression [34] disrupted integrin adhesion in the fly wing, presumably through imbalanced responses to an accumulation of the same phosphoinositide pool. PI3KC2 and Mtm family members in vertebrates have been associated with antagonistic functions related to regulation of traffic to the plasma membrane. PI3KC2 isoforms are required to promote while overexpression of MTM1 impairs GLUT4 trafficking [20,35] and integrin-mediated cell motility [21,36]. Together, the observations point to a broad and conserved relationship for PI3KC2/Mtm co-regulation at the plasma membrane.

How might PI3KC2 and Mtm co-regulate integrin trafficking? One possibility is that the cycle of phosphoinositides co-regulated by PI3KC2/Mtm tunes the balance between endocytic-exocytic flux. The strong genetic interaction between *mtm* and *Pi3K68D*, in conjunction with Pi3KC2 ability to create PI(3)P *in vivo* [18,20–23], supports the possibility that Pi3K68D could generate a PI(3)P substrate pool acted on by Mtm phosphatase. Alternatively, Pi3K68D could act more distantly on an interrelated phosphoinositide pool. We envision that Pi3K68D mediates early endocytic trafficking, tethering or sorting of integrin-containing vesicles. The integrin detected on large inclusions in *mtm*-depleted and XLMTM muscles in flies and humans, respectively, and evidence that *mtm* promotes membrane tubulation from PI(3)P compartments [18,37], point to an Mtm/MTM1 role in membrane efflux for delivery of integrin to the plasma membrane. Mtm phosphatase could act to promote recycling or to negatively regulate retention, for example, through a PI(3)P-mediated fusion of integrin-containing vesicles with endosomes-lysosomes. An accumulation of β1-integrin on enlarged, perinuclear compartments has been observed with certain genetic manipulations in non-muscle cells. These results raise the possibility that normal Mtm phosphatase activity functions antagonistically to Rab21 GTPase or in concert with PKCε kinase, Rab11 and/or Arf6 GTPase, respectively, to control redelivery of β-integrin to the plasma membrane [38–40]. We found that class III PI3K, *Vps34*, also contributes to integrin localization upon myofiber remodeling, but with no effect on integrin-containing inclusions. A requirement for class III Pi3K could be at a shared step with the early endosomal Rab5 GTPase shown to be involved in integrin turnover at larval MTJs [6]. Thus, regulation of distinct PI(3)P pools is important for differential regulation of integrin endosomal trafficking, whereby Pi3KC2 and Mtm are dedicated to specific paired antagonistic functions.

We discovered that *mtm* is required in muscle for both integrin-mediated adhesions and T-tubule organization. The T-tubule requirement for *mtm* was similar to but not as severe as that for *amph*, the sole homolog of human *AMPH2* that is also associated with centronuclear myopathy [41]. However, unlike *mtm*, null alleles of *amph* did not share a defect of myofiber detachment. Despite localization of βPS-integrin at T-tubules, and the dual requirements for *mtm*, we found that normal integrin adhesions and abnormal βPS-integrin localization on inclusions are independent of T-tubule organization. This suggests that *mtm* may serve a common function for integrin turnover and T-tubule formation at a shared precursor compartment, for example, at recycling endosomes, or alternatively, act independently at two distinct sites. β-integrin, Dlg and Amph are known to functionally interact at postsynaptic junctions [42–44], and MTMR2 has been shown to interact with Dlg1/SAP-97 and Dlg4/PSD-95 to promote postsynaptic function [45,46]. Thus, the shared accumulation of βPS-integrin, Dlg and Amph on central membrane inclusions in *mtm*-depleted myofibers, and their elimination with *Pi3K68D* co-depletion, points to a possible role for a PI3KC2/Mtm pathway in endocytic recycling at neuromuscular junctions, as well as at MTJs.

Many of the defects observed in *mtm* mutant muscle parallel those associated with the human disease, XLMTM, demonstrating that the fly offers a tractable model for the cellular basis of centronuclear myopathy. Importantly, the discovery that *mtm* broadly regulates βPS-integrin turnover through endocytic trafficking led us to uncover a previously untested defect in β1-integrin localization in human XLMTM myofibers. Normal myofiber organization and function rely on integrin adhesions in vertebrate muscle [2,3,31,47]. Thus, disruption of integrin regulation provides a basis for aspects of the severity of myofiber disorganization and dysfunction observed in XLMTM. The conservation between fly *mtm* and human *MTM1* functions brings further significance to the potent interaction demonstrated between *mtm* and class II *Pi3K68D* for integrin regulation in flies. Whereas Class I and III PI3-kinases have been the focus of intense study as potential therapeutic targets of specific inhibitory compounds, the Class II PI3-kinases have received little attention. The knowledge of PI3KC2 contributions to specific MTM pathways is significant towards motivating similar studies for potential strategies addressing MTM-related disease.

Mtm is the single fly homolog related to both human MTM1 and MTMR2, and human *MTMR2* expression was able to rescue integrin-related defects in *mtm*-depleted fly myofibers. An *mtm* pathway function in endocytic trafficking is therefore relevant to a more general understanding of the cell biological functions employed by MTM subfamily members. Mutations in *MTMR2* associated with CMT4B neuropathy affect the morphology and function of myelinating Schwann cells [11], which like myofibers, share features of having an extensive plasma membrane and a reliance on integrin adhesions [48]. The regulation of integrin trafficking under the control of a conserved PI3KC2/Mtm pathway may be an important mechanism for controlling cell compartmentalization more broadly in different contexts, and relevant to different MTM-related human disease.

Materials and Methods

Ethics statement

Human samples were obtained and used as per institutional IRB accepted protocol.

Fly genetics

Flies were reared at 25°C, unless stated. Stocks used include: $mtm^{\Delta 77}$, $mtm^{z2\text{-}4747}$ and RNAi hairpins *w; UAS-IR-mtm*$^{3\text{-}1}$ and *w; UAS-IR-mtm*$^{3\text{-}5}$ interchangeably or in combination when "2x IR-mtm" noted, *w; UAS-mtm:GFP*^{7} and *w; UAS-GFP:MTMR2* [18]; *UAS-IR-Pi3K68D*^{v16240} and *UAS-IR-Vps34*^{v100296} (VDRC); *UAS-Vps34-KD*^{m8} [49]; *How*^{24B}*-GAL4*, *DMef2-GAL4*, *UAS-Dcr2; DMef2-GAL4*, *UAS-2xeGFP*^{AH2}, *mys*^{1} and *mys*^{ts1} (Bloomington); *if*^{3} (F. Schöck); *Ubi-βPS-integrin:YFP* [6]; *amph*^{26} [28]; *w, dlg1:GFP*^{YC0005} (FlyTrap, [50]); *UAS-GFP:LAMP* [51]; *UAS-GFP:Rab5* and *UAS-GFP:myc:2xFYVE* [52]; *UAS-GFP:Rab7* [53]; *UAS-mRFP:PH-FAPP1* (G. Polevoy and J. Brill). *UAS-GFP:Atg8a* [54] and *Ubi-Talin:GFP* [55]. To reduce βPS-integrin function, *mys*^{1}*/mys*^{ts1} flies raised at permissive 22°C were shifted to 29°C at pupation until lethality at pharate stage. To reduce *mtm* function specifically during pupation, *UAS-EGFP/+; DMef2-GAL4, tubulin-Gal80*^{ts}/+ and *UAS-EGFP, UAS-IR-mtm*$^{3.1}$*/+; DMef2-GAL4, tubulin-Gal80*^{ts}/+ flies raised at permissive 18°C were shifted to 29°C at 2 days after pupation until pharate stage. To reduce *mtm* function in adults,

UAS-Dcr2; Mef2-GAL4/UAS-EGFP and *UAS-Dcr2; Mef2-GAL4/UAS-EGFP, UAS-IRmtm$^{3.1}$* flies raised at permissive 18°C were shifted to 29°C at eclosion until adults were analyzed at 6 or 10 days old.

Muscle preparations and immunofluorescence

Staged pharate adults were removed from pupal case fastened to double-sided tape and pinned on a sylgard covered petri dish in dissecting buffer (5 mM HEPES, 128 mM NaCl, 2 mM KCl, 4 mM $MgCl_2$, 36 mM sucrose, pH 7.2). Abdomens were opened with longitudinal and two lateral incisions, pinned flat, washed and fixed 30 min. (3.7% formaldehyde, 50 mM EGTA, PBS), washed, unpinned and blocked (0.3% bovine serum albuminum, 2% goat serum, 0.1% Triton, PBS), incubated with primary antibody overnight 4°C, washed (0.1% Triton PBS), reblocked and incubated overnight 4°C with Alexa-secondary antibodies (Molecular Probes), counterstained with phalloidin for F-actin and DNA as needed, and mounted in Fluorsave. Antibodies included Amph Ra29 (C. O'Kane), Dlg 4F3 and βPS-integrin CG.6G11 (Developmental Studies Hybridoma Bank), α-tubulin (Sigma-Aldrich), Zormin B1 (B. Bullard), muscle myosin (D. Kiehart), αPS2-integrin 7A10 [56], anti-Rabenosyn-5 [57] and KDEL (Babraham Institute). Propidium iodide (PI) staining was done on tissue. Pharate adult and adult abdomens were dissected in dissection buffer as above, washed once with PBS 0.2% BSA and maintained in 0.3 mg/ml PI final concentration in PBS 0.2% BSA throughout imaging. Images of abdomen fillets were taken with a Leica DMI 6000B inverted microscope using semi-apochromat 5× objective (N.A. 0.15), of live IOMs with a Zeiss Axiovert 200M using a LD-Plan NeoFluar 20× (N.A. 0.4) objective and of individual myofibers with FV1000 Olympus point scanning confocal using 60× Plan Apo N (N.A. 1.2) and 100× Plan Apo (N.A. 1.45) objectives. Exported TIFFs were handled by Adobe Photoshop or ImageJ software.

Timelapse microscopy

White pupae were positioned on double-sided tape on a coverslip, placed in a petri dish with water-soaked filter and incubated at 25°C. At each time point, the coverslip was flipped over for imaging on Leica DMI 6000B, as above.

FRAP

FRAP was carried out as described [6] in living 3rd instar larvae. Integrin:YFP was heterozygous (Int/+) in all experiments. A total of 21 and 19 individual FRAP experiments from multiple larvae were carried out for *int*/+ and *mtm$^{z2-4747}$/mtm$^{\Delta 77}$;int*/+ respectively.

Electron microscopy

Pharate adults dissected and pinned flat were fixed 1 hr. RT (0.1 M sodium phosphate, 3% paraformaldehyde, 2% glutaraldehyde, 2 mM sodium EGTA, 0.1 M sucrose, pH 7.2), postfixed 1 hr. (1% osmium tetroxide in 0.1 M cacodylate buffer) and stained 1 hr. (1% uranyl acetate). Abdomen fillets were embedded in epoxy resin and 70 nm sections were collected on Formvar and carbon-coated copper grids.

Viability and flight assays

To assay viability, pre-cleared vials were counted for surviving adults, dead adults post-eclosion on food and mid-eclosion, dead pharates and dead pupae at 13 or 17 days after egg laying. Flies 1–6 days old were tested for flight at least 24 hours after CO_2 anesthesia, by releasing 12 females in a 2 L cylinder (50.8 cm high). Flies that landed below 0.6 L (14.6 cm) were scored flightless.

Human muscle studies

8 mM cryosections were obtained from muscle biopsies from 3 genetically confirmed cases of XLMTM and age matched cases without obvious histopathology (Carsten Bonnemann), per institutional IRB accepted protocol. Sections were stained using manufacturers instructions (NovoLink kit, Novocastra) and as previously described [14] using primary antibodies to beta1D integrin (Chemicon; 1:25) and dystroglycan (Novocastra; 1:20).

Statistical analyses

Visual quantification was made for number of IOMs in tergites 3 and 4, number of detached IOMs per abdomen, number of IOMs displaying βPS-integrin costameres or βPS-integrin- or Dlg-marked inclusions, and number of nuclei per IOM. ImageJ software was used to draw and measure nuclei distance to IOM midline and sarcomere length. CellProfiler was used to segment and quantify nuclei morphology. Statistical analysis in Prism software used to determine mean, standard error and Student's t-test, where possible.

Genotypes

Full genotypes used are as shown in Figure Legends and as follows:

Figure 1. (D,G,H,I,J) Control, *UAS-EGFP/+; DMef2-GAL4/+*. (D′,G′,H′,I,J) RNAi: *UAS-EGFP, UAS-IR-mtm$^{3.1}$/+; DMef2-GAL4/+*. (C) 24B-GAL4. Control: *UAS-EGFP/24B-GAL4*. RNAi: *UAS-EGFP, UAS-IR-mtm$^{3.1}$/24B-GAL4*. RNAi with *mtm* cDNA: *UAS-mtm:EGFP, UAS-IR-mtm$^{3.1}$/24B-GAL4*. RNAi with human *MTMR2* cDNA: *UAS-EGFP:huMTMR2, UAS-IR-mtm$^{3.1}$/24B-GAL4*. DMef2-GAL4. Control: *UAS-EGFP/+; DMef2-GAL4, UAS-LacZ/+*. RNAi: *UAS-EGFP/+; DMef2-GAL4, UAS-IR-mtm$^{3.5}$/+*. (E, F). 24B-GAL4: Control: *UAS-EGFP/24B-GAL4*. 1x RNAi: *UAS-IR-mtm$^{3.1}$/24B-GAL4*. 2x RNAi: *UAS-IR-mtm$^{3.1}$/24B-GAL4; UAS-IR-mtm$^{3.5}$/+*. DMef2-GAL4. Control: *UAS-EGFP/+; DMef2-GAL4/+*. 1x RNAi: *UAS-IR-mtm$^{3.1}$/+; DMef2-GAL4/+*. 2x RNAi: *UAS-IR-mtm$^{3.1}$/+; DMef2-GAL4/UAS-IR-mtm$^{3.5}$*.

Figure 2. (B,C,D,E) Control: *UAS-EGFP/+; DMef2-GAL4/+*. (B′,C′,D′,E′) RNAi: *UAS-EGFP, UAS-IR-mtm$^{3.1}$/+; DMef2-GAL4/+*. (F) Control: *Ubi-βPS-integrin:YFP/+*. mutants: *mtm$^{\Delta 77}$/mtm$^{z2-4747}$/Ubi-βPS-integrin:YFP*. (G,H) *dlg1:GFP*. (I) Control: *UAS-Dcr2; Mef2-GAL4/UAS-EGFP*. RNAi: *UAS-Dcr2; Mef2-GAL4/UAS-EGFP, UAS-IRmtm$^{3.1}$*.

Figure 3. (B,C) Control: *UAS-EGFP/+; DMef2-GAL4/+*. RNAi: *UAS-EGFP, UAS-IR-mtm$^{3.1}$/+; DMef2-GAL4/+*. (D, D′) *amph^{26}*. (E) *amph^{26}/amph^{26}, UAS-IR-mtm$^{3.1}$/+; DMef2-GAL4/+*. (F) *mys^{1}/mys^{ts1}*.

Figure 4. (A) Control: *UAS-GFP:LAMP/+; DMef2-GAL4/+*. (A′–A″) RNAi: *UAS-GFP:LAMP, UAS-IR-mtm$^{3.1}$/+; DMef2-GAL4/+*. (B) Control: *UAS-GFP:Rab5/+; DMef2-GAL4, UAS-lacZ/+*. (B′–B″) RNAi: *UAS-GFP:Rab5/+; DMef2-GAL4, UAS-IRmtm$^{3.5}$/+*. (C,D) Control: *UAS-GFP:myc:2XFYVE/+; DMef2-GAL4/+*. (C′,D′,C′,D″′) RNAi: *UAS-GFP:myc:2XFYVE, UAS-IR-mtm$^{3.1}$/+; DMef2-GAL4/+*.

Figure 5. (B,C,D,E,F) Control: *UAS-EGFP/+; DMef2-GAL4, UAS-lacZ/+*. RNAi: *UAS-EGFP/+; DMef2-GAL4, UAS-IR-mtm$^{3.5}$/+*. (A,A′,B,C′,C″D,E′,E″,F) Single RNAi: *DMef2-GAL4, UAS-lacZ/UAS-IR-Pi3K68D* or *UAS-IR-Vps34/+; DMef2-GAL4, UAS-lacZ/+*. *mtm* co-RNAi: *DMef2-GAL4, UAS-IR-mtm$^{3.5}$/UAS-IR-Pi3K68D* or *UAS-IR-Vps34/+; DMef2-GAL4, UAS-IR-mtm$^{3.5}$/+*.

Supporting Information

Figure S1 Mtm maintains myofiber attachments and visceral muscle function. (A) RT-PCR of *mtm* RNAi depletion detected in whole adult thorax. *Rp32L* control RT-PCR from same tissue. (B) Western Blot of Mtm:GFP (anti-GFP) knockdown with muscle-targeted *mtm* RNAi and control protein (anti-α-tubulin) detected in whole pharate adults. (C) Normal third instar larval body wall muscle in control and (C′) *mtm* knockdown animals, with two copies of RNAi hairpin. Muscle myosin. (D–D′) Pharate ventral abdominal muscles. Arrowheads, detached PLMs. F-actin. (A,B,C) Control: *UAS-EGFP/+; DMef2-GAL4/+*. (A′,B,C′) *mtm* RNAi: *UAS-EGFP, UAS-IR-mtm$^{3.1}$/+; DMef2-GAL4/+*. (E–F) Ventral PLMs quantified in filleted abdomens with 24B-GAL4 or DMef2-GAL4 expression of 1 or 2 copies of *mtm* RNAi hairpins. (E) Number of ventral PLMs present, including detached PLMs. (F) Number of present but detached ventral PLMs. (G) Normal tubular shape of testis ensheathed by visceral muscle (green). Asterisk, testis tip. *24B-GAL4/UAS-EGFP*, green; F-actin, red; DNA, blue. (G′) Abnormally round, short testis indicative of visceral muscle defect. Arrowhead, testis base attached to seminal vesicle. *24B-GAL4/UAS-EGFP, UAS-IR-mtm$^{3.1}$*. Scale bar 200 μm, except F–F′ 50 μm.
Found at: doi:10.1371/journal.pgen.1001295.s001 (3.43 MB TIF)

Figure S2 Mtm is unessential for myofiber cell viability and normal sarcomere assembly. (A) Normal nuclei morphology in (A) control and (A′) *mtm* RNAi IOMs. Myofiber nuclei analyzed for condensation (DAPI intensity) and nuclei size (perimeter) were similarly normal in control and *mtm* RNAi IOMs. Mean, s.d. for nuclei measured from 5–7 experiments. (B–B′) Nuclei (blue; white arrowhead positions) in pharate IOMs do not stain with propidium iodide (red, PI) in either control (B) or *mtm* RNAi (B′) conditions. GFP, green; DNA, blue. (C) Nuclei (blue) in IOMs of 1 day old adults were permeable to propidium iodide (red, PI; yellow arrowheads) in both control (C) and *mtm* RNAi (C′) conditions. GFP, green; DNA, blue. (D–D′) Transmission electron microscopy of IOM cross-sections, showing mitochondria with intact membranes and normal size and morphology. (E–E′) Normal microtubule organization between myofibrils and in perinuclear space. α-tubulin, green; DNA, blue. (F–F′) Normal Zormin sarcomere localization at repeating Z-lines. (G–G′) Normal Z-line and sarcomere ultrastructure. (H) Normal sarcomere length (μm), as measured in Zormin-stained myofibrils. IOMs, control: *UAS-EGFP/+; DMef2-GAL4/+*. RNAi: *UAS-EGFP, UAS-IR-mtm$^{3.1}$/+; DMef2-GAL4/+*. Scale bars 10 μm, except D–D′, G–G′ 1 μm.
Found at: doi:10.1371/journal.pgen.1001295.s002 (4.96 MB TIF)

Figure S3 Mtm is required for transverse tubule formation and organization. (A–A′) Amph protein (green, top; single channel, bottom) localized at T-tubules. (A′) Higher density of longitudinal and lack of transversal membrane elements in *mtm*-depleted muscle. F-actin, red (top). (B–B′) Dlg protein (green, top; single channel, bottom) showed similar localization to Amph at T-tubules. Zormin, red (top). (C) Schematic of dorsal IOM. Cell surface (top; integrin adhesions shown in grey) and cut-away central section of myofiber (bottom; nuclei shown in center), indicating the orientation of longitudinal and transversal T-tubules (green) in the central periphery regions in images shown (blue box). (D–D′) Transmission electron microscopy shows radial spokes of transverse-tubule membranes (arrowheads) in myofiber cross-sections of control muscles (D), undetected in *mtm*-depleted IOMs (D′). IOMs, control: *UAS-EGFP/+; DMef2-GAL4/+*. RNAi: *UAS-EGFP, UAS-IR-mtm$^{3.1}$/+; DMef2-GAL4/+*. Schematic indicating peripheral central region of myofiber where microscopy z-sections imaged. Scale bars 10 μm, except D–D′ 1 μm.
Found at: doi:10.1371/journal.pgen.1001295.s003 (4.47 MB TIF)

Figure S4 βPS-integrin inclusions specifically accumulate due to a requirement for an *mtm* function during metamorphosis. (A–A′) Normal αPS2-integrin localization at IOM MTJs (arrows; green and single channels) and undetected on Dlg-containing inclusions (red) with *mtm* RNAi. Control: *UAS-EGFP/+; DMef2-GAL4, UAS-lacZ/+*. RNAi: *UAS-EGFP/+; DMef2-GAL4, UAS-IR-mtm$^{3.5}$/+*. (B–B′) Normal GFP:Talin localization at IOM MTJs (arrows; green and single channels) and undetected on βPS-integrin inclusions (red) with *mtm* RNAi. DNA, blue. Control: *Ubi-GFP:Talin/+; DMef2-GAL4, UAS-lacZ/+*. RNAi: *Ubi-GFP:Talin/+; DMef2-GAL4, UAS-IR-mtm$^{3.5}$/+*. (C-C′) Normal βPS-integrin localization at larval MTJs (arrows; green and single channels), along peripheral cell surface and in small internal punctae in *OreR* and *mtm$^{\Delta 77}$/mtm$^{z2-4747}$* third instar larvae. F-actin, red; DNA, blue. (D–D′) *UAS-EGFP,UAS-IR-mtm$^{3.1}$/+; DMef2-GAL4/+* pharates. (D) Normal IOM attachments when flies raised continuously at 18°C, due to low levels of GAL4 activity. (D′) Pharate adults show IOM detachment (arrowheads) when upshifted from 18°C to 29°C for 1–2 days, due to *mtm* RNAi during pupal stages. EGFP. (E) Percent pharate adults with one or more detached IOMS. (F–F′) *UAS-EGFP,UAS-IR-mtm$^{3.1}$/+; DMef2-GAL4, tub>Gal80^{ts}/+* pharates. (F) Normal βPS-integrin localization (red, and single channel) in pharate adult IOM in flies raised continuously at 18°C, due to GAL80^{ts}-inhibited GAL4 activity. (F′) Abnormal integrin inclusions (arrowheads) in IOMs of flies raised at 18° until pupation, then upshifted to 29°C for 3 days, due to *mtm* RNAi during pupal stages. GFP, green; DNA, blue. (G) Percent of IOMs with integrin-containing inclusions. Scale bars 10 μm, except D–D′ 200 μm.
Found at: doi:10.1371/journal.pgen.1001295.s004 (5.75 MB TIF)

Figure S5 Membrane inclusions in *mtm*-depleted myofibers are an endosomal-related compartment. (A) Co-localization of βPS-integrin and Amph increased along longitudinal T-tubules in IOM central periphery regions with *mtm* knockdown, as determined by Pearson correlation. (B–B″) βPS-integrin (red) and Amph (green) infrequently co-localized (arrowheads) in control IOMs (B). With *mtm* RNAi, βPS-integrin and Amph became continuously co-localized along longitudinal T-tubules in central periphery (B′, βPS-integrin single channel at right) and showed punctuated co-localization along inclusions (B″, arrowheads). Control: *dlg1:GFP; DMef2-GAL4, UAS-lacZ/+*. RNAi: *dlg1:GFP; DMef2-GAL4, UAS-IR-mtm$^{3.5}$/+*. (C) Schematic of dorsal IOM. Cell surface (top; integrin adhesions shown in grey) and cut-away central section of myofiber (bottom; nuclei shown in center), indicating the orientation of longitudinal and transversal T-tubules (green) in the central periphery regions in images shown (blue box). (D) *amph^{26}* null mutant. Dlg (white) detected in discontinuous longitudinal patches between myofibrils and missing from transversal elements of T-tubules, and normal aligned nuclei (blue) in myofiber perinuclear area. (E–E′) Normal KDEL (green) distribution in IOMs localized to sarcoplasmic reticulum between myofibrils and perinuclear endoplasmic reticulum, but undetected on abnormal inclusions with *mtm* RNAi. Control: *UAS-EGFP/+; DMef2-GAL4/+*. RNAi: *UAS-EGFP, UAS-IR-mtm$^{3.1}$/+; DMef2-GAL4/+*. (F–F′) Normal mRFP:PH-FAPP1 (green) distribution indicating trans-Golgi network in IOMs localized between but not on abnormal inclusions with *mtm* RNAi. Control: *UAS-EGFP/UAS-mRFP:PH-FAPP1; DMef2-GAL4/+*. RNAi: *UAS-EGFP, UAS-IR-mtm$^{3.1}$/UAS-mRFP:PH-FAPP1; DMef2-GAL4/+*. (E–F′) F-actin and cytoplasmic GFP, co-imaged and pseudocolored red. (G–G′)

Few small GFP:Atg8a punctae (green), indicative of autophagosomes, with similar distribution in control and *mtm* RNAi IOMs, and not detected on inclusions. Control: *UAS-GFP:Atg8a*/+; *DMef2-GAL4*, *UAS-lacZ*/+. RNAi: *UAS-GFP:Atg8a*/+; *DMef2-GAL4*, *UAS-IR-mtm*$^{3.5}$/+. (H–H′) Small punctae positive for Rbsn5 (green) throughout IOMs, with infrequent Rbsn5 co-localized with integrin (red) on inclusions with *mtm* RNAi (H′). Control: *UAS-EGFP*/+; *DMef2-GAL4*/+. RNAi: *UAS-EGFP*, *UAS-IR-mtm*$^{3.1}$/+; *DMef2-GAL4*/+. EGFP not depicted. (I) In control IOMs, GFP:Rab7 (green) detected as small particles throughout myofiber periphery and in larger clusters in perinuclear region. (I′) In *mtm* RNAi IOMs, GFP:Rab7 is absent from periphery and does not colocalize on inclusions. Control: *UAS-GFP:Rab7*/+; *DMef2-GAL4*, *UAS-lacZ*/+. RNAi: *UAS-GFP:Rab7*/+; *DMef2-GAL4*, *UAS-IR-mtm*$^{3.5}$/+. βPS-integrin, red; DNA, blue. Scale bars 10 μm.
Found at: doi:10.1371/journal.pgen.1001295.s005 (6.43 MB TIF)

Figure S6 Lethality and Dlg inclusions with muscle-specific *mtm* RNAi are rescued by *Pi3K68D* co-depletion. (A) Percent viable and lethal staged progeny at 17 days after staged egg lays for *Dcr2; DMef2-GAL4* single and double RNAi hairpin conditions, as shown; ≥3 experiments. Disruption of class II or III Pi3-kinases alone (*IR-Pi3K68D* hairpin and *Vps34-KD*, kinase dead) did not alter viability. Co-disruption of *Pi3K68D* or *Vps34* with *mtm* co-RNAi, respectively, restored or enhanced lethality and delayed development. (B) RT-PCR of *Pi3K68D* depletion and *GAPDH2* control detected in adult abdomens with DMef2-GAL4 muscle-driven *Pi3K68D* RNAi. (C) Percentage of IOMs with severity of T-tubule defects, as detected by Dlg. White, transverse elements detected throughout >50% of each myofiber; grey, transverse elements detected in 10–50% of each myofiber; dark grey, transverse elements detected in <10% of each myofiber. Pooled from 2 experiments. (D) Percentage of flightless adults, aged 1–6 days old, from ≥5 experiments (semi-lethality prevented equivalent numbers from *IRmtm*, *Vps34-KD*). (E) Percentage of IOMs that contain Dlg detected along abnormal inclusions, for single (light grey, 0%) and *mtm* double (dark grey) RNAi conditions as shown. Genotypes as in Figure 5, in addition to *UAS-Vps34-KD*. (F–F′) Pharate abdominal muscles, F-actin. (F) *IR-Atg1* alone and (F′) with *mtm* co-RNAi. Arrowheads, detached IOMs. (G–G′) Sarcolemmal βPS-integrin no longer detected at costameres; (G) *IR-Atg1* alone and (G′) with *mtm* co-RNAi. (H–H′) βPS-integrin central *z*-sections; (H) no inclusions detected with *IR-Atg1* alone and (H′) inclusions present with *mtm* co-RNAi. (F–H′) Control: *UAS-IR-Atg1*/+; *DMef2-GAL4*, *UAS-lacZ*/+. RNAi: *UAS-IR-Atg1*/+; *DMef2-GAL4*, *UAS-IR-mtm*$^{3.5}$/+. Scale bars, F–F′ 200 μm, G–H′ 10 μm.
Found at: doi:10.1371/journal.pgen.1001295.s006 (2.92 MB TIF)

Acknowledgments

We thank D. Bilder, J. Brill, B. Bullard, T. Bunch, L. Cooley, M. Gonzalez-Gaitan, D. Kiehart, H. Krämer, T. Neufeld, C. O'Kane, F. Schöck, Developmental Studies Hybridoma Bank, and the stock centers Bloomington, FlyTrap, and VDRC for reagents. We thank members of the Kiger lab, R. Firtel, and C. Weaver for comments. We are grateful to T. Meerloo for technical assistance with electron microscopy preparation and to M. Farquhar for use of the CMM Electron Microscope Facility. Imaging was conducted in part in the UCSD Neuroscience Microscopy Shared Facility.

Author Contributions

Conceived and designed the experiments: IR GT JJD AK. Performed the experiments: IR LY JJD. Analyzed the data: IR LY GT JJD AK. Contributed reagents/materials/analysis tools: IR AK. Wrote the paper: IR AK.

References

1. Brower DL (2003) Platelets with wings: the maturation of Drosophila integrin biology. Curr Opin Cell Biol 15: 607–613.
2. Mayer U, Saher G, Fassler R, Bornemann A, Echtermeyer F, et al. (1997) Absence of integrin alpha 7 causes a novel form of muscular dystrophy. Nat Genet 17: 318–323.
3. Volk T, Fessler LI, Fessler JH (1990) A role for integrin in the formation of sarcomeric cytoarchitecture. Cell 63: 525–536.
4. Caswell PT, Vadrevu S, Norman JC (2009) Integrins: masters and slaves of endocytic transport. Nat Rev Mol Cell Biol 10: 843–853.
5. Kaisto T, Rahkila P, Marjomaki V, Parton RG, Metsikko K (1999) Endocytosis in skeletal muscle fibers. Exp Cell Res 253: 551–560.
6. Yuan L, Fairchild MJ, Perkins AD, Tanentzapf G (2010) Analysis of integrin turnover in fly myotendinous junctions. J Cell Sci 123: 939–946.
7. Di Paolo G, De Camilli P (2006) Phosphoinositides in cell regulation and membrane dynamics. Nature 443: 651–657.
8. Nicot AS, Laporte J (2008) Endosomal phosphoinositides and human diseases. Traffic 9: 1240–1249.
9. Buj-Bello A, Laugel V, Messaddeq N, Zahreddine H, Laporte J, et al. (2002) The lipid phosphatase myotubularin is essential for skeletal muscle maintenance but not for myogenesis in mice. Proc Natl Acad Sci U S A 99: 15060–15065.
10. Laporte J, Hu LJ, Kretz C, Mandel JL, Kioschis P, et al. (1996) A gene mutated in X-linked myotubular myopathy defines a new putative tyrosine phosphatase family conserved in yeast. Nat Genet 13: 175–182.
11. Bolino A, Muglia M, Conforti FL, LeGuern E, Salih MA, et al. (2000) Charcot-Marie-Tooth type 4B is caused by mutations in the gene encoding myotubularin-related protein-2. Nat Genet 25: 17–19.
12. Berger P, Bonneick S, Willi S, Wymann M, Suter U (2002) Loss of phosphatase activity in myotubularin-related protein 2 is associated with Charcot-Marie-Tooth disease type 4B1. Hum Mol Genet 11: 1569–1579.
13. Cao C, Backer JM, Laporte J, Bedrick EJ, Wandinger-Ness A (2008) Sequential actions of myotubularin lipid phosphatases regulate endosomal PI(3)P and growth factor receptor trafficking. Mol Biol Cell 19: 3334–3346.
14. Dowling JJ, Vreede AP, Low SE, Gibbs EM, Kuwada JY, et al. (2009) Loss of myotubularin function results in T-tubule disorganization in zebrafish and human myotubular myopathy. PLoS Genet 5: e1000372. doi:10.1371/journal.pgen.1000372.
15. Kim SA, Taylor GS, Torgersen KM, Dixon JE (2002) Myotubularin and MTMR2, phosphatidylinositol 3-phosphatases mutated in myotubular myopathy and type 4B Charcot-Marie-Tooth disease. J Biol Chem 277: 4526–4531.
16. Taylor GS, Maehama T, Dixon JE (2000) Inaugural article: myotubularin, a protein tyrosine phosphatase mutated in myotubular myopathy, dephosphorylates the lipid second messenger, phosphatidylinositol 3-phosphate. Proc Natl Acad Sci U S A 97: 8910–8915.
17. Tsujita K, Itoh T, Ijuin T, Yamamoto A, Shisheva A, et al. (2004) Myotubularin regulates the function of the late endosome through the gram domain-phosphatidylinositol 3,5-bisphosphate interaction. J Biol Chem 279: 13817–13824.
18. Velichkova M, Juan J, Kadandale P, Jean S, Ribeiro I, et al. (2010) Drosophila Mtm and class II PI3K coregulate a PI(3)P pool with cortical and endolysosomal functions. J Cell Biol 190: 407–425.
19. Lindmo K, Stenmark H (2006) Regulation of membrane traffic by phosphoinositide 3-kinases. J Cell Sci 119: 605–614.
20. Falasca M, Hughes WE, Dominguez V, Sala G, Fostira F, et al. (2007) The role of phosphoinositide 3-kinase C2alpha in insulin signaling. J Biol Chem 282: 28226–28236.
21. Maffucci T, Cooke FT, Foster FM, Traer CJ, Fry MJ, et al. (2005) Class II phosphoinositide 3-kinase defines a novel signaling pathway in cell migration. J Cell Biol 169: 789–799.
22. Srivastava S, Di L, Zhdanova O, Li Z, Vardhana S, et al. (2009) The class II phosphatidylinositol 3 kinase C2beta is required for the activation of the K+ channel KCa3.1 and CD4 T-cells. Mol Biol Cell 20: 3783–3791.
23. Wen PJ, Osborne SL, Morrow IC, Parton RG, Domin J, et al. (2008) Ca2+-regulated pool of phosphatidylinositol-3-phosphate produced by phosphatidylinositol 3-kinase C2alpha on neurosecretory vesicles. Mol Biol Cell 19: 5593–5603.
24. Roy S, VijayRaghavan K (1998) Patterning muscles using organizers: larval muscle templates and adult myoblasts actively interact to pattern the dorsal longitudinal flight muscles of Drosophila. J Cell Biol 141: 1135–1145.
25. Wasser M, Bte Osman Z, Chia W (2007) EAST and Chromator control the destruction and remodeling of muscles during Drosophila metamorphosis. Dev Biol 307: 380–393.
26. Kozopas KM, Samos CH, Nusse R (1998) DWnt-2, a Drosophila Wnt gene required for the development of the male reproductive tract, specifies a sexually dimorphic cell fate. Genes Dev 12: 1155–1165.
27. Al-Qusairi L, Weiss N, Toussaint A, Berbey C, Messaddeq N, et al. (2009) T-tubule disorganization and defective excitation-contraction coupling in muscle

fibers lacking myotubularin lipid phosphatase. Proc Natl Acad Sci U S A 106: 18763–18768.
28. Razzaq A, Robinson IM, McMahon HT, Skepper JN, Su Y, et al. (2001) Amphiphysin is necessary for organization of the excitation-contraction coupling machinery of muscles, but not for synaptic vesicle endocytosis in Drosophila. Genes Dev 15: 2967–2979.
29. Wilcox M, DiAntonio A, Leptin M (1989) The function of PS integrins in Drosophila wing morphogenesis. Development 107: 891–897.
30. Walsh EP, Brown NH (1998) A screen to identify Drosophila genes required for integrin-mediated adhesion. Genetics 150: 791–805.
31. Ervasti JM (2003) Costameres: the Achilles' heel of Herculean muscle. J Biol Chem 278: 13591–13594.
32. Sparrow JC, Schock F (2009) The initial steps of myofibril assembly: integrins pave the way. Nat Rev Mol Cell Biol 10: 293–298.
33. Perkins AD, Ellis SJ, Asghari P, Shamsian A, Moore ED, et al. (2010) Integrin-mediated adhesion maintains sarcomeric integrity. Dev Biol 338: 15–27.
34. MacDougall LK, Gagou ME, Leevers SJ, Hafen E, Waterfield MD (2004) Targeted expression of the class II phosphoinositide 3-kinase in Drosophila melanogaster reveals lipid kinase-dependent effects on patterning and interactions with receptor signaling pathways. Mol Cell Biol 24: 796–808.
35. Chaussade C, Pirola L, Bonnafous S, Blondeau F, Brenz-Verca S, et al. (2003) Expression of myotubularin by an adenoviral vector demonstrates its function as a phosphatidylinositol 3-phosphate [PtdIns(3)P] phosphatase in muscle cell lines: involvement of PtdIns(3)P in insulin-stimulated glucose transport. Mol Endocrinol 17: 2448–2460.
36. Domin J, Harper L, Aubyn D, Wheeler M, Florey O, et al. (2005) The class II phosphoinositide 3-kinase PI3K-C2beta regulates cell migration by a PtdIns3P dependent mechanism. J Cell Physiol 205: 452–462.
37. Fili N, Calleja V, Woscholski R, Parker PJ, Larijani B (2006) Compartmental signal modulation: Endosomal phosphatidylinositol 3-phosphate controls endosome morphology and selective cargo sorting. Proc Natl Acad Sci U S A 103: 15473–15478.
38. Ivaska J, Whelan RD, Watson R, Parker PJ (2002) PKC epsilon controls the traffic of beta1 integrins in motile cells. EMBO J 21: 3608–3619.
39. Pellinen T, Arjonen A, Vuoriluoto K, Kallio K, Fransen JA, et al. (2006) Small GTPase Rab21 regulates cell adhesion and controls endosomal traffic of beta1-integrins. J Cell Biol 173: 767–780.
40. Powelka AM, Sun J, Li J, Gao M, Shaw LM, et al. (2004) Stimulation-dependent recycling of integrin beta1 regulated by ARF6 and Rab11. Traffic 5: 20–36.
41. Nicot AS, Toussaint A, Tosch V, Kretz C, Wallgren-Pettersson C, et al. (2007) Mutations in amphiphysin 2 (BIN1) disrupt interaction with dynamin 2 and cause autosomal recessive centronuclear myopathy. Nat Genet 39: 1134–1139.
42. Beumer K, Matthies HJ, Bradshaw A, Broadie K (2002) Integrins regulate DLG/FAS2 via a CaM kinase II-dependent pathway to mediate synapse elaboration and stabilization during postembryonic development. Development 129: 3381–3391.
43. Mathew D, Popescu A, Budnik V (2003) Drosophila amphiphysin functions during synaptic Fasciclin II membrane cycling. J Neurosci 23: 10710–10716.
44. Regalado MP, Terry-Lorenzo RT, Waites CL, Garner CC, Malenka RC (2006) Transsynaptic signaling by postsynaptic synapse-associated protein 97. J Neurosci 26: 2343–2357.
45. Bolino A, Bolis A, Previtali SC, Dina G, Bussini S, et al. (2004) Disruption of Mtmr2 produces CMT4B1-like neuropathy with myelin outfolding and impaired spermatogenesis. J Cell Biol 167: 711–721.
46. Lee HW, Kim Y, Han K, Kim H, Kim E (2010) The phosphoinositide 3-phosphatase MTMR2 interacts with PSD-95 and maintains excitatory synapses by modulating endosomal traffic. J Neurosci 30: 5508–5518.
47. Hayashi YK, Chou FL, Engvall E, Ogawa M, Matsuda C, et al. (1998) Mutations in the integrin alpha7 gene cause congenital myopathy. Nat Genet 19: 94–97.
48. Barros CS, Nguyen T, Spencer KS, Nishiyama A, Colognato H, et al. (2009) Beta1 integrins are required for normal CNS myelination and promote AKT-dependent myelin outgrowth. Development 136: 2717–2724.
49. Juhasz G, Hill JH, Yan Y, Sass M, Baehrecke EH, et al. (2008) The class III PI(3)K Vps34 promotes autophagy and endocytosis but not TOR signaling in Drosophila. J Cell Biol 181: 655–666.
50. Quinones-Coello AT, Petrella LN, Ayers K, Melillo A, Mazzalupo S, et al. (2007) Exploring strategies for protein trapping in Drosophila. Genetics 175: 1089–1104.
51. Pulipparacharuvil S, Akbar MA, Ray S, Sevrioukov EA, Haberman AS, et al. (2005) Drosophila Vps16A is required for trafficking to lysosomes and biogenesis of pigment granules. J Cell Sci 118: 3663–3673.
52. Wucherpfennig T, Wilsch-Brauninger M, Gonzalez-Gaitan M (2003) Role of Drosophila Rab5 during endosomal trafficking at the synapse and evoked neurotransmitter release. J Cell Biol 161: 609–624.
53. Entchev EV, Schwabedissen A, Gonzalez-Gaitan M (2000) Gradient formation of the TGF-beta homolog Dpp. Cell 103: 981–991.
54. Scott RC, Schuldiner O, Neufeld TP (2004) Role and regulation of starvation-induced autophagy in the Drosophila fat body. Dev Cell 7: 167–178.
55. Tanentzapf G, Brown NH (2006) An interaction between integrin and the talin FERM domain mediates integrin activation but not linkage to the cytoskeleton. Nat Cell Biol 8: 601–606.
56. Bogaert T, Brown N, Wilcox M (1987) The Drosophila PS2 antigen is an invertebrate integrin that, like the fibronectin receptor, becomes localized to muscle attachments. Cell 51: 929–940.
57. Morrison HA, Dionne H, Rusten TE, Brech A, Fisher WW, et al. (2008) Regulation of early endosomal entry by the Drosophila tumor suppressors Rabenosyn and Vps45. Mol Biol Cell 19: 4167–4176.